

10-27-2018

On the Asymmetry Between Upward and Downward Field-Aligned Currents Interacting With the Ionosphere

A. V. Streltsov
Embry-Riddle Aeronautical University, streltsa@erau.edu

Follow this and additional works at: <https://commons.erau.edu/publication>



Part of the [Atmospheric Sciences Commons](#)

Scholarly Commons Citation

Streltsov, A. V. (2018). On the asymmetry between upward and downward field-aligned currents interacting with the ionosphere. *Journal of Geophysical Research: Space Physics*, 123, 9275–9285. <https://doi.org/10.1029/2018JA025826>

This Article is brought to you for free and open access by Scholarly Commons. It has been accepted for inclusion in Publications by an authorized administrator of Scholarly Commons. For more information, please contact commons@erau.edu.

RESEARCH ARTICLE

10.1029/2018JA025826

Key Points:

- The nonlinear stage of the magnetosphere-ionosphere interactions conducted by the electromagnetic ULF waves at high altitudes is investigated
- We demonstrate that MI interactions can generate FAC system with significantly different upward and downward currents
- The ionospheric parameters leading to the formation of the “black” aurora have been identified

Correspondence to:

 A. V. Streltsov,
 streltsa@erau.edu

Citation:

Streltsov, A. V. (2018). On the asymmetry between upward and downward field-aligned currents interacting with the ionosphere. *Journal of Geophysical Research: Space Physics*, 123, 9275–9285. <https://doi.org/10.1029/2018JA025826>

Received 27 JUN 2018

Accepted 22 OCT 2018

Accepted article online 27 OCT 2018

Published online 20 NOV 2018

On the Asymmetry Between Upward and Downward Field-Aligned Currents Interacting With the Ionosphere

A. V. Streltsov^{1,2} 

¹Department of Physical Sciences, Embry-Riddle Aeronautical University, Daytona Beach, FL, USA, ²National Academy of Sciences at Space Vehicles Directorate, Air Force Research Laboratory/RVBXC, Kirtland AFB, Albuquerque, NM, USA

Abstract The paper presents results from the numerical study of the magnetosphere-ionosphere interactions driven by the large-scale electric field in the magnetically conjugate, high-latitude regions of northern and southern hemispheres. Simulations of the two-fluid MHD model demonstrate that these interactions can lead to a generation of a system of small-scale, intense field-aligned currents with a significant difference in size and amplitude between the upward and downward currents. In particular, in both hemispheres, the downward currents (where the electrons are flowing from the ionosphere) become more narrow and intense than the adjacent upward currents. At high latitudes, the field-aligned currents are closely related to the discrete auroral arcs. The fact that this mechanism produces very narrow and intense downward currents embedded into the broader upward current regions makes it relevant to the explanation of the “black” auroral arcs appearing as narrow, dark strips embedded in the broad luminous background.

1. Introduction

Magnetosphere-ionosphere interactions at high latitudes include exchange of mass, energy, and momentum between the relatively cold and dense, strongly collisional ionospheric plasma and more energetic, less dense and almost completely collisionless plasma in the magnetosphere. The main part of that exchange is conducted by the electromagnetic waves and field-aligned currents (FACs) in the ULF frequency range. Therefore, understanding of spatial structures/distributions, temporal dynamics, and physical mechanisms providing generation and amplification of ULF waves in the near-Earth space is essential for the understanding of basic physics of magnetosphere-ionosphere coupling.

In general, magnetosphere-ionosphere interactions lead to a great number of wave and particle phenomena in the ULF frequency range with very different spatial and temporal scales, levels of intensity, frequencies, and the “favorable” conditions for occurrence. The key element of these interactions is the change in the ionospheric conductivity by the fluxes of electrons carried by FACs from/to the magnetosphere and the active ionospheric feedback on the structure and amplitude of the incident currents. The positive ionospheric feedback is the essence of the ionospheric feedback instability (IFI) introduced by Atkinson (1970). IFI develops when the shear Alfvén waves (and the corresponding FACs) form a standing pattern in one of two major resonator cavities in the magnetosphere. One of them is the global magnetospheric resonator, formed by the entire closed magnetic flux tube bounded by the ionosphere in two hemispheres (Cummings et al., 1969; Samson et al., 1992). The other is the ionospheric Alfvén resonator formed by the part of the magnetic flux tube between the ionosphere and a strong gradient in the background Alfvén speed at the altitude $\approx 1 R_E$ (Polyakov & Rapoport, 1981).

IFI has been extensively studied for more than 40 years in both resonators (e.g., Lysak, 1991; Miura & Sato, 1980; Pokhotelov et al., 2000, 2001; Russell et al., 2013; Streltsov & Lotko, 2005; Trakhtengertz & Feldstein, 1981, 1991; Watanabe et al., 1993). These studies demonstrate that IFI is a strongly nonlinear process which can produce different wave, current, and density structures, depending on the background parameters in the magnetosphere-ionosphere system. This paper presents results from the numerical investigation of the feedback mechanism in the global magnetospheric resonator leading to the formation of a system of FACs with a strong asymmetry in spatial sizes and amplitudes between upward and downward currents. This asymmetry

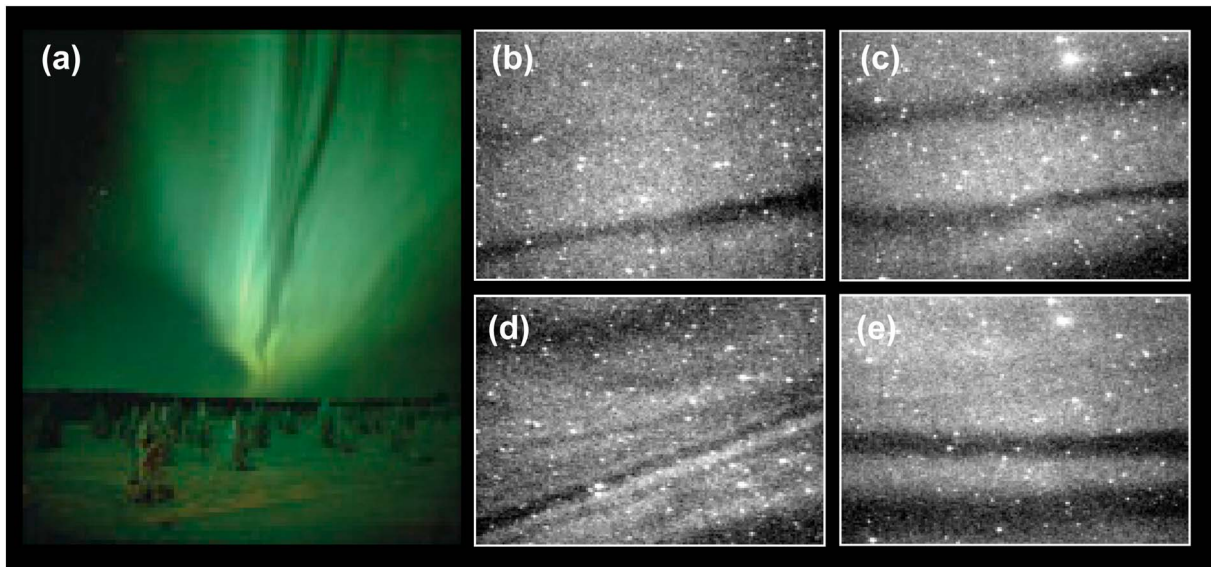


Figure 1. Images of the black aurora. (a) is adapted from Marklund et al. (2011), and (b)–(e) are adapted from Trondsen and Cogger (1997).

can explain the geophysical phenomena called a *black aurora*, which appears in the auroral zone as a narrow dark strip “sandwiched” between two broad luminous regions.

The black aurora had been studied from the ground and from satellites for more than 20 years, but its quantitative and self-consistent picture has not been developed yet. The main features distinguishing the black aurora from a dark region between two adjacent bright discrete arcs in a multiple arc system are (1) its transverse size is much smaller than the width of the adjacent bright regions, and (2) there is a very sharp boundary (no transition region) between the dark and bright regions. These features are illustrated in Figure 1, showing one image of the black aurora taken from Marklund et al. (2011) and four images from Trondsen and Cogger (1997).

These images show relatively narrow homogeneous dark strips on the broad luminous background, and the goal of this paper is to explain this particular topology of the observations. No attempts to reproduce these images in the quantitative details will be made. In general, the black aurora may demonstrate other geometric forms similar to the normal, bright aurora, in particular, curls and vortex chains (Trondsen & Cogger, 1997). These forms also will not be discussed in the paper because our model is two-dimensional: One dimension is along the ambient magnetic field, and another is in the north-south direction. Thus, the main questions which this study will answer are (1) Why is the black aurora narrower than the adjacent bright aurora? (2) What information does this feature provide about parameters of the coupled magnetosphere-ionosphere system?

Bright auroral arcs are produced by the fluxes of magnetospheric electrons flowing toward the ionosphere in a form of the upward FACs. Electrons can be accelerated inside the upward current by the parallel electric field (or the parallel potential drop) caused by several linear and nonlinear mechanisms related to the magnitude and transverse size of the current (e.g., Goertz & Boswell, 1979; Hasegawa, 1976; Lysak & Dum, 1983; Stasiewicz et al., 2000). In that case, it is reasonable to assume that the black aurora is related to the downward current, where the electrons are moving from the ionosphere as has been shown by Marklund et al. (1994, 1997, 2011) using data from the Freja and Cluster satellites. In some studies, the black aurora is identified as a dark lane in a diffuse aurora, and the diffuse aurora is associated with pitch angle scattering rather than FACs. For example, Trondsen and Cogger (1997) state that “... ‘black aurora’ is a lack of emission in a small, well-defined region within an otherwise uniform, diffuse background, or within auroras exhibiting a degree of shear behavior intermediate between that of diffuse and discrete aurora.” The present simulations do not address this situation, and therefore, they do not cover all cases of the black aurora. The main questions addressed in this study can be reformulated in terms of FACs as (1) What is the physical mechanism making the downward currents more narrow and intense than the adjacent upward current? and (2) What are the geomagnetic conditions activating and facilitating this mechanism?

Marklund et al. (2001) suggest that the structure of the electron fluxes and the electric field observed on satellites in the upward current channel is explained by the interaction of this current with the ionosphere. Another point of view has been expressed by Gustavsson et al. (2008): Using data from the EISCAT radar and optical observations of the black aurora, these authors suggest that “... the mechanism causing black aurora is most probably active in the magnetosphere rather than close to Earth.”

The results presented in this paper support the suggestion made by Marklund et al. (2001) that the main mechanism leading to the narrowing of the downward current channel is indeed interaction between FACs and the ionosphere. We also make the next step in the development of this concept and provide a self-consistent, dynamical picture of this process. In particular, our simulations demonstrate that the IFI, driven by the electric field in the ionosphere, can produce inside the global magnetosphere resonator a system of FACs with a strong asymmetry between upward and downward currents as it is observed in the black aurora. The study is based on the reduced two-fluid MHD model discussed together with the geophysical conditions leading to the development of IFI in the next section of the paper.

2. Model

The model used in this study is similar to the one used by Streltsov et al. (2012), and it contains the magnetospheric and ionospheric parts. The magnetospheric part describes shear Alfvén waves (Chmyrev et al., 1988) and consists of the electron momentum equation, the density continuity equation, and the current continuity equation:

$$\frac{\partial v_{\parallel e}}{\partial t} + v_{\parallel e} \nabla_{\parallel} v_{\parallel e} + \frac{e}{m_e} E_{\parallel} + \frac{1}{m_e n_0} \nabla_{\parallel} (n T_e) = -\nu_e v_{\parallel e}, \quad (1)$$

$$\frac{\partial n}{\partial t} + \nabla \cdot (n v_{\parallel e} \hat{\mathbf{b}}) = 0, \quad (2)$$

$$\nabla \cdot j_{\parallel} \hat{\mathbf{b}} + \frac{1}{\mu_0} \nabla \cdot \left(\frac{1}{c^2} + \frac{1}{v_A^2} \right) \frac{\partial \mathbf{E}_{\perp}}{\partial t} = 0. \quad (3)$$

Here the subscripts \parallel and \perp denote vector components in the directions parallel and perpendicular to $\hat{\mathbf{b}} = \mathbf{B}_0/B_0$, respectively; $v_{\parallel e}$ is the parallel component of the electron velocity; T_e is the background electron temperature, c is the speed of light; $v_A = B_0/\sqrt{\mu_0 n_0 m_i}$ is the Alfvén speed; and ν_e is the electron collision frequency. The wave magnetic field is defined as $\mathbf{B} = \nabla \times \mathbf{A}$, where $\mathbf{A} = A_{\parallel} \hat{\mathbf{b}}$ is the vector potential; the parallel current density is defined as $j_{\parallel} = -\nabla_{\perp}^2 A_{\parallel}$; and the electric field is defined as $\mathbf{E} = -\nabla \phi - \frac{\partial \mathbf{A}}{\partial t}$, where ϕ is the scalar potential. The introduction of scalar and vector potentials automatically satisfies the Faraday’s law and the condition $\nabla \cdot \mathbf{B} = 0$.

This study focuses on two-dimensional auroral structures (like the ones shown in Figure 1) associated with FAC sheets extended in one direction perpendicular to the ambient magnetic field and localized in another perpendicular direction. To model such structures, equations (1)–(3) have been implemented numerically in a two-dimensional, axisymmetric dipole region, bounded by $L_1 = 4.6$ and $L_2 = 5.2$ magnetic shells. The ionospheric footprint of the central magnetic shell of the domain ($L = 4.9$) corresponds to the magnetic latitude of the High Frequency Active Aurora Program facility in Gakona, Alaska, where various discrete auroral arcs have been regularly observed (e.g., Streltsov et al., 2011).

The ionospheric boundaries of the domain are set at 100-km altitude. Because the height of the conducting portion of the ionosphere is always much less than the parallel wavelength of ULF waves, the conducting bottom of the ionosphere can be considered as a narrow slab where the density and the electric field are relatively uniform. In that case, the simplest mathematical form of the ionospheric part of the model can be given by two equations connecting the perpendicular electric field, E_{\perp} , and the plasma density, n_e , in the ionosphere with the FAC density, j_{\parallel} . One is the Poisson equation, derived by integrating the current continuity equation $\nabla \cdot \mathbf{j} = 0$ over the effective thickness of the ionospheric E region ($h \approx 10 - 20$ km):

$$\nabla \cdot (\Sigma_p \mathbf{E}_{\perp}) = \pm j_{\parallel}. \quad (4)$$

Another is the ionospheric density continuity equation:

$$\frac{\partial n_E}{\partial t} = \frac{j_{\parallel}}{eh} + \alpha n_E^2 - \alpha n_{E0}^2. \quad (5)$$

Here, $\Sigma_p = M_p n_E h e / \cos \psi$; $M_p = 10^4 \text{ m}^2/\text{sV}$ is the ion Pedersen mobility (the Hall conductivity is not included in (4) due to the two-dimensionality of the considered problem); e is the elementary charge; ψ is the angle between the normal to the ionosphere and $L = 4.9$ dipole magnetic field line at 100-km altitude. In (4), the “+” sign should be used in the southern hemisphere, and “−” sign should be used in the northern hemisphere. The term αn_E^2 in the right-hand side of (5) represents losses due to the recombination ($\alpha = 3 \times 10^{-7} \text{ cm}^3/\text{s}$ is the coefficient of recombination); and the term αn_{E0}^2 represents the unperturbed source of the ionospheric plasma, which provides an equilibrium state of the ionosphere, n_{E0} .

The model can be advanced further by including additional ionization of the ionosphere by the energetic electrons precipitated in the upward current channel or by the effects of the neutral wind. None of these effects changes the essence of the positive ionospheric feedback, which is the main focus of this study.

Recently, Sydorenko and Rankin (2017) demonstrate with numerical simulations that under some particular conditions, the instability can be saturated by the inhomogeneity in the collision frequency between ions and neutrals in the ionospheric E region. This inhomogeneity causes shear in the ion velocity with altitude that can “smooth out” the localized density/conductivity disturbances in the ionosphere. This particular effect has been rigorously studied by Trakhtengertz and Feldstein (1981, 1984, 1991), who demonstrated that it changes the growth rate and the threshold of the instability but does not prevent IFI from the development. These papers show that even when the ionospheric parameters significantly change with the altitude, the conducting bottom of the ionosphere still can be considered as the height-integrated slab. However, in that case, the boundary conditions, the threshold values of the electric field, and the growth rate of the instability will be different compared with the case when the collision frequency is considered to be homogeneous over the height of the conducting layer. In particular, Trakhtengertz and Feldstein (1991) provide the boundary conditions in the ionosphere (equations (A6)–(A11)) which should be used to describe the active ionospheric feedback when the inhomogeneity of the ion-neutral collision frequency is taken into account. Also, Trakhtengertz and Feldstein (1991) provide expressions for the threshold electric field and the growth rate of the instability, which give quite reasonable values for the parameters observed in the high-latitude ionosphere.

The IFI has been extensively studied for more than 40 years (e.g., Atkinson, 1970; Lysak, 1991; Lysak & Song, 2002; Miura & Sato, 1980; Pokhotelov et al., 2000, 2001; Russell et al., 2013; Sato, 1978; Streltsov & Lotko, 2005; Trakhtengertz & Feldstein, 1981, 1991; Watanabe et al., 1993), and the important conclusion from these studies is that IFI occurs only when and where the conditions for its development are satisfied. These conditions include the large-scale electric field in the ionosphere and the low ionospheric density in the E region. The large-scale electric field provides the energy for the intensification of the small-scale ULF waves and FACs due to the so-called *over reflection* from the ionosphere (e.g., Lysak & Song, 2002). The low ionospheric density (a) provides a low conductance of the E region, which allows the electric field generated by the dynamo processes in the equatorial magnetosphere to penetrate into the ionosphere and (b) reduces the effects of the recombination, which saturate the instability.

This conclusion from theoretical studies is supported by the observations showing that intense ULF waves with characteristic frequencies of magnetospheric resonators are observed with ground magnetometers, sounding rockets, and satellites predominantly during the nighttime, particularly, in a winter season and in the vicinity of discrete auroral arcs. Observations from the Freja satellite reported by Marklund et al. (1997) also show that the occurrence and the magnitude of the localized electric fields associated with the black aurora maximize when the ionospheric conductivity is minimal, namely, during the winter solstice and near the local midnight.

In summary, more than 40 years of theoretical and experimental studies confirmed by numerous observations provide a solid basis to conclude that IFI is a well-established geophysical process existing in the Earth’s magnetosphere-ionosphere system. When the necessary conditions for the instability are satisfied, IFI can be successfully modeled with equations (4) and (5) by considering the ionosphere as a narrow conducting slab.

2.1. Background Parameters

The background magnetic field is considered to be dipole, defined as $B_0 = B_* (1 + 3 \sin^2 \lambda)^{1/2} / r^3$, where $B_* = 31,000$ nT, r is the radial distance measured in Earths radii ($R_E = 6,371.2$ km), and λ is the magnetic latitude.

The density inside the domain is modeled as $n_0(L, \mu) = n_{01}(L) n_{02}(\mu)$, where $L = r / \sin^2 \theta$ is the coordinate in the direction normal to the dipole magnetic shells ($\theta = \pi/2 - \lambda$) and $\mu = \cos \theta / r^2$ is the coordinate along the ambient magnetic field (Cumplings et al., 1969). The function $n_{01}(L)$ defines the density distribution across the ambient magnetic field, and the function $n_{02}(\mu)$ defines the density along the ambient magnetic field, and it is chosen in a form similar to the one used by Streltsov et al. (2012):

$$n_{02}(\mu) = \begin{cases} a_1 (r(\mu) - r_1) + a_2, & r_1 < r(\mu) < r_2 \\ b_1 e^{-20(r(\mu)-r_2)} + b_2 r^{-3}(\mu) + b_3, & r(\mu) > r_2. \end{cases}$$

Here $r(\mu)$ is a radial distance to the point on the $L_0 = (L_1 + L_2)/2 = 4.90$ magnetic field line with that particular μ value, $r_1 = 1 + 100/R_E$, $r_2 = 1 + 320/R_E$, and the constants a_1, a_2, b_1, b_2 , and b_3 are chosen to provide some prescribed values of plasma density at the altitudes 100 km, 320 km, and in the equatorial magnetosphere. The main problem with the ionospheric density at high latitudes is its large variability, particularly during active geomagnetic periods, when strong FACs interact with the ionosphere and change the conductivity/density in broad ranges. For example, the magnitude of the plasma density inside the E region can be in the range from 2.5×10^3 to 3×10^5 cm^{-3} depending on the geomagnetic conditions. In this study, we chose the parameters for the plasma density as 10^4 cm^{-3} at 100 km and 3×10^5 cm^{-3} at 320 km.

The value of the plasma density in the equatorial magnetosphere is not a very important parameter of the model. That value affects the magnitude of the eigenfrequency of standing Alfvén waves in the global magnetospheric resonator, but because the Alfvén speed is quite high near the equator, simulations show that even variation of the plasma density in that region by a factor of 2 or 3 does not change results significantly. In this paper, we follow Streltsov et al. (2012) and assume the magnitude of the plasma density in the equatorial magnetosphere of 129 cm^{-3} .

Equation (4) shows that the background electric field in the ionosphere will generate FACs if $\nabla_{\perp} \cdot (\Sigma_{p0} \mathbf{E}_{0\perp}) \neq 0$. Which means, that in the case of a current-free equilibrium, the ionospheric density defines the structure of $\mathbf{E}_{0\perp}$ in the ionosphere. And because we assume that there is no constant parallel potential drops in the magnetosphere, the ionospheric electric field is mapped equipotentially along the ambient magnetic field in the magnetosphere. Therefore, the ionospheric density defines the structure of the background electric field inside the entire computational domain.

We will consider two cases: (1) when the ionospheric density/conductivity is uniform across the magnetic field and (2) when there is a density cavity. These two cases are described with the formula

$$n_{01}(L) = \begin{cases} \frac{1+\kappa}{2} + \frac{1-\kappa}{2} \cos\left(\frac{2\pi(L-L_0)}{\Delta L}\right), & \text{if } |L - L_0| \leq \Delta L/2, \\ \kappa, & \text{if } |L - L_0| > \Delta L/2. \end{cases} \quad (6)$$

Here $L_0 = (L_1 + L_2)/2$; parameter ΔL defines the size of the cavity, and the parameter κ defines how much the magnitude of the density at the edges of the cavity is greater/smaller than the density magnitude inside. If $\kappa = 1$, then the plasma is homogeneous ($n_{01}(L) \equiv 1$).

It should be mentioned here that even in the homogeneous case ($\Sigma_{p0} \equiv \text{constant}$), the perpendicular electric field in the ionosphere still has a small gradient in the direction perpendicular to the magnetic field. It came from the fact that the L component of the operator $\nabla_{\perp} \cdot (\Sigma_{p0} \mathbf{E}_{0\perp})$ has the form $(1/h_L) \partial(E_{0L} h_L \Sigma_{p0}) / \partial L$, where $h_L(L)$ is the metric factor associated with the dipole L coordinate and $E_{0L} \propto \Sigma_{p0} / h_L(L)$ to satisfy the current-free equilibrium condition.

Electron and ion temperatures are defined as $T_{e,i} = T_{e,i}^* (n_*/n_0)$, where the constants $T_e^* = 2$ eV, $T_i^* = 2$ eV, and $n_* = 129$ cm^{-3} represent corresponding quantities in the equatorial plane on the $L = 4.9$ magnetic shell. This relation between n_0 and $T_{e,i}$ nullifies the parallel gradient in plasma pressure and provides the MHD equilibrium in the dipole magnetic field.

3. Results and Discussion

We model the development of the IFI produced by the electric field with a maximum amplitude of 10 mV/m in the homogeneous ionosphere with the density magnitude of 10^4 cm^{-3} (corresponds to $\Sigma_{p0} = 0.33$ mho).

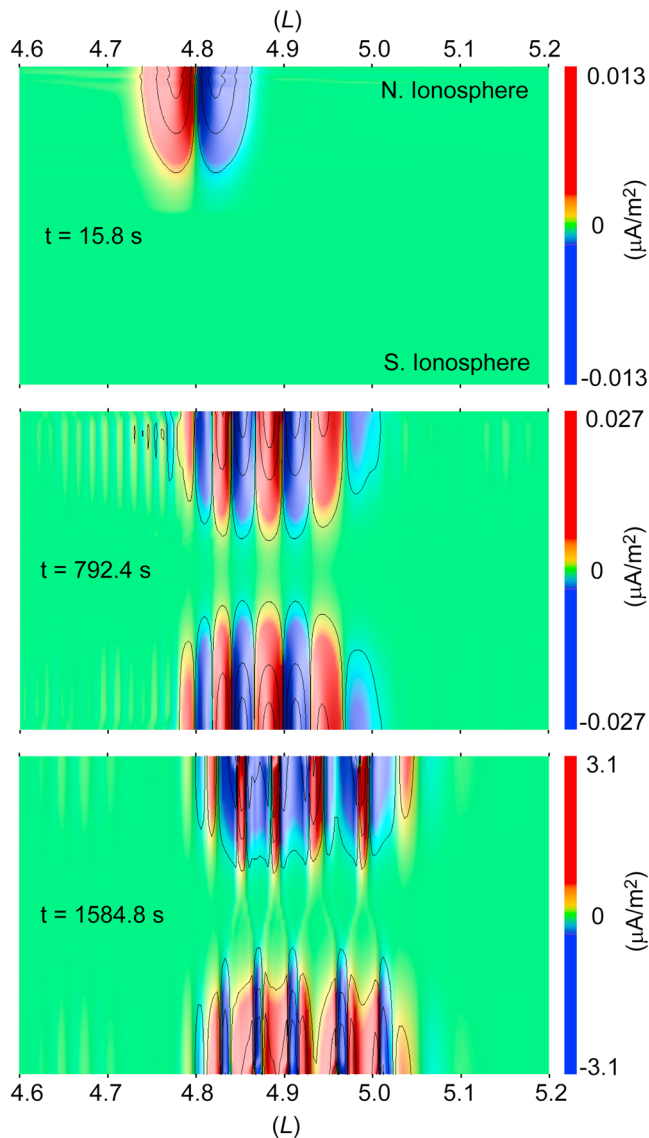


Figure 2. Snapshots of the parallel current density, j_{\parallel} , taken from the simulations with a background ionospheric conductivity $\Sigma_{p0} = 0.33$ mho and the 10-mV/m electric field at $t = 15.8$, 792.4, and 1,584.8 s.

The instability is triggered by a small-scale, Gaussian-shape disturbance of the ionospheric density in the northern hemisphere at $L = 4.8$ with a transverse size of 10% of the size of the domain (corresponds to ≈ 20 km at 100-km altitude) and a magnitude of 10% of the background. These parameters are close to the parameters of the disturbances produced by the artificial heating of the ionosphere with the High Frequency Active Aurora Program transmitter (Streltsov et al., 2011). Several test simulations showed that parameters of the initial density disturbance have a relatively limited effect on the instability development. They affect the time when the instability reaches its saturated state but do not affect the final amplitudes or sizes of the nonlinear structures.

The initial disturbance was placed slightly off the center of the computational domain because the development of the instability is governed by the dynamics of the ionospheric density disturbance, which is defined by the ions flowing in the direction of the background electric field (in this case, in the positive L direction). Thus, several test simulations showed that when $E_{0\perp} \approx 10$ mV/m, the instability initiated near $L = 4.8$ reaches its saturated state near $L = 4.9$.

Figure 2 shows three snapshots of the parallel current density in the simulation at $t = 15.8$, 792.4, and 1,584.8 s. The red color marks “positive” FACs flowing in the direction of the ambient magnetic field (from the southern to northern hemispheres), and the blue color marks “negative” FACs flowing in the opposite direction. From the ionospheric point of view, the same positive current is the upward current in the southern hemisphere and the downward current in the northern hemisphere. This feature is very important because these currents change the ionospheric conductivities in the opposite way: The upward current increases the conductivity, and the downward current decreases it.

The $t = 15.8$ -s snapshot in Figure 2 illustrates the initial FACs generated in the northern hemisphere and propagating along the magnetic field. The $t = 792.4$ -s snapshot illustrates a situation when the instability is in its linear stage, which means that the disturbances of the electric field and conductivity are much less than the background values, and the instability develops a system of relatively symmetrical upward and downward FACs. The $t = 1,584.8$ -s snapshot illustrates the nonlinear stage of the instability, namely, when it produces system of FACs with a strong asymmetry in structure and amplitude between the upward and downward currents. In both hemispheres, the downward currents became more narrow and intense than the upward currents.

To illustrate the downward currents becoming more narrow in more detail, j_{\parallel} , E_{\perp} , and Σ_p in the northern and southern hemispheres are shown in Figures 3a–3c at $t = 792.4$ s and in Figures 3d–3f at $t = 1,584.8$ s. Figures 3g–3j show the same quantities in the southern hemisphere only. Figures 3a–3c illustrate the linear stage of the instability, when the amplitude of the disturbed electric field and the ionospheric conductivity are much less than the amplitude of the corresponding background quantities. At that time, the instability produces periodic fluctuations in the ionospheric conductivity, electric field, and the parallel current density with equal amplitude and spatial sizes of the depletions and enhancements. This stage of IFI has been well-studied in a number of theoretical papers (e.g., Lysak, 1991; Pokhotelov et al., 2000; Trakhtengertz & Feldstein, 1991), and the basic physical mechanism generating the FACs are variations in the ionospheric density in the presence of a large-scale electric field. In that case, the maximum amplitudes of the FACs collocate with the gradients in the conductivity/density, as shown in Figures 3a–3c.

Figures 3d–3f illustrate a strongly nonlinear phase of the instability, when the magnitudes of the disturbed parts of the electric field and plasma density became comparable or even larger than the magnitudes of the background quantities. At this time, the behavior of the fields and currents changes compared with the linear

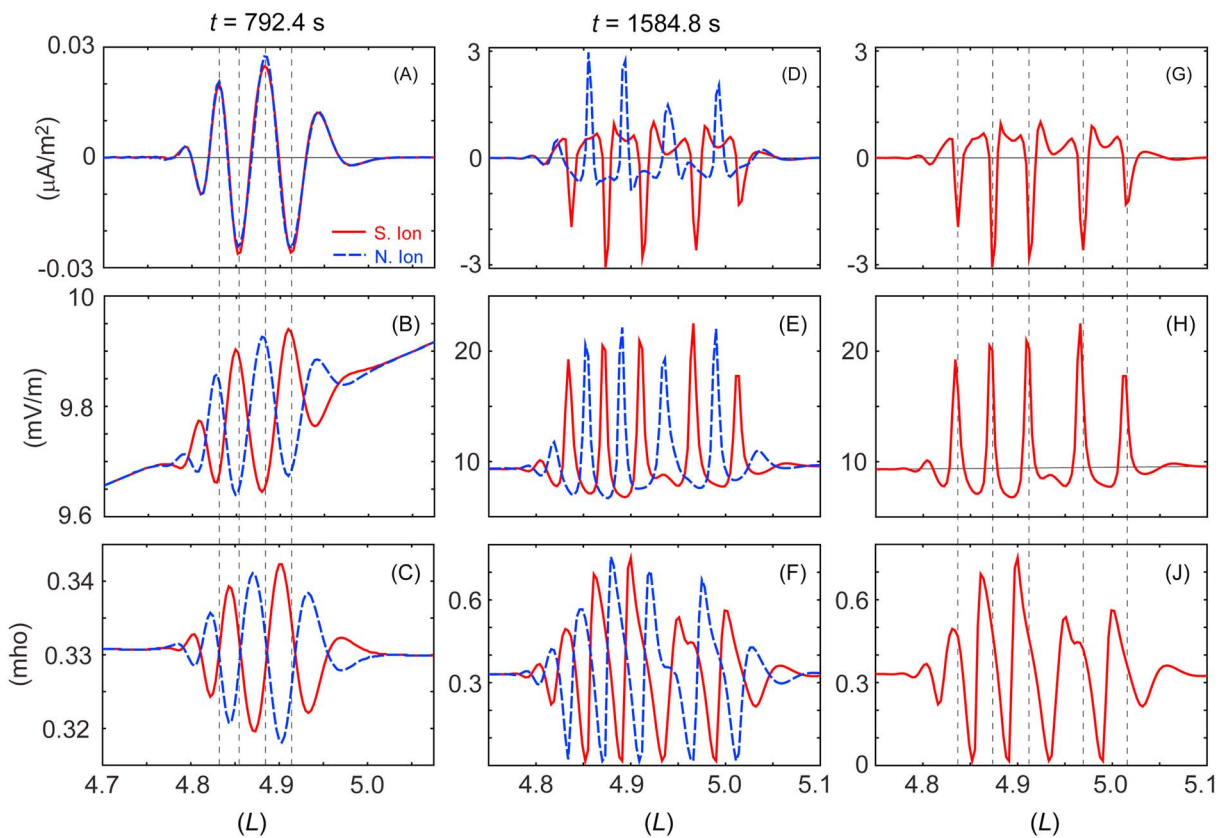


Figure 3. (a–c) Parallel current density, perpendicular electric field, and Pedersen conductivity in the northern (blue-dashed lines) and southern (red solid lines) hemispheres in the simulations with the ionospheric conductivity $\Sigma_{p0} = 0.33$ mho and the 10-mV/m electric field at $t = 792.4$ s. (d–f) The same quantities in the same simulations at $t = 1,584.8$ s. (g–i) The same quantities as shown in (d)–(f) in the southern hemisphere only.

phase. In particular, in both hemispheres, the amplitude of the downward FACs increases and their perpendicular size decreases compared with the amplitude and size of the upward FACs. Figures 3d and 3g show that the amplitudes of the small-scale, downward FACs in both hemispheres are ≈ 3 times larger than the amplitudes of the adjacent upward currents, and their perpendicular sizes are ≈ 3 times less than the sizes of the upward currents.

Figures 3g and 3h also show that the peaks in the perpendicular electric field are very close but do not collocate exactly with the corresponding peaks in the downward FAC density. This feature is very similar to the relation between the very strong localized perpendicular electric field and the decrease in the flux of the downgoing electrons observed by the Cluster 3 satellite above the auroral oval at the altitude $\approx 1 R_E$ (see Figure 3 in Marklund et al., 2011).

It should be mentioned here that spikes in the parallel current density associated with the large conductivity gradients have also been observed in simulations of the IFI by Lysak and Song (2002; their Figure 4). But in that case, these spikes were attached to the broader region of the FACs of the same sign, whereas in our case, these spikes are isolated. So it is worth emphasizing as shown in Figure 3g, the positive and negative currents are separated not with relatively smooth transition regions but with very sharp gradients. This result suggests that there should be a very sharp contrast (no “gray” area) between the black aurora (downward current channel) and the adjacent luminous regions (upward currents). And this is, indeed, a very distinctive feature of the black aurora illustrated in Figure 1.

The main factor changing the instability development in the nonlinear stage is the fact that the magnetic FACs generated by the electric field in one hemisphere acts as a strong external driver, producing significant effect on the density and the electric field in another hemisphere. This stage can be characterized by strong nonlinear interactions between two ionospheric feedback instabilities occurring simultaneously in the magnetically conjugate hemispheres connected by a system of magnetic FACs. This can be called a *double*

ionospheric feedback instability, and it is very different from the IFI inside the ionospheric Alfvén resonator, where the instability develops inside the cavity formed by the active ionosphere on one side and a strong gradient in the background Alfvén speed on the other.

Behavior of the downward currents shown in Figures 2 and 3 is also different from the behavior of a single, isolated downward current interacting with the ionosphere. Observations by the Cluster satellites (Marklund et al., 2001) demonstrate that a single downward current interacting with the ionosphere increases its width and decreases its amplitude with time. That dynamic has been reproduced with simulations of the magnetosphere-ionosphere model very similar to the one presented in this study by Streltsov and Marklund (2006; hereafter SM06). The main differences between the setups of the simulations in Streltsov and Marklund (2006) and reported in this paper are (1) SM06 considers interaction between a single isolated downward current (without adjacent downward currents) and the ionosphere, (2) SM06 considers interaction between the current and the ionosphere only in one hemisphere, (3) SM06 does not consider any background electric field in the ionosphere, and (4) SM06 does not include the IFI (no global magnetospheric resonator).

These differences emphasize our conclusion that the IFI driven by the large-scale electric field in both hemispheres can produce a system of FACs with a strong asymmetry between downward and upward currents, as the one observed in the black aurora. The asymmetry originates from the fact that the upward FAC increases the ionospheric conductivity and the downward current decreases it. To maintain the closure of the FACs through the ionosphere, the electric field increases where the conductivity decreases and decreases where the conductivity increases. Thus, the amplitude of the perpendicular electric field and the current density increases with time in the downward current channel. Because the amplitude of the downward current becomes greater than the amplitude of the upward current, the width of the downward current channel becomes smaller than the width of the upward current to maintain the current continuity in the system.

This simplified explanation does not take into account the fact that the FAC changes the rate of the density variation in the ionosphere and not the density itself (see equation (5)). Also, it does not take into account the perpendicular motion of small-scale current, density, and the electric field structures in the ionosphere. It does not include effects of the FACs generated in the conjugate hemisphere and any of the nonlinear effects, which are expected to be significant because the amplitudes of the disturbances of the density and the electric field are comparable with the background values. However, this explanation provides a simple qualitative insight into the complex nonlinear behavior of the coupled magnetosphere-ionosphere system.

The results illustrated in Figures 2 and 3 are obtained assuming homogeneous plasma and relatively homogeneous electric field in the ionosphere. Both these quantities are inhomogeneous across the ambient magnetic field in the real ionosphere, and the importance of that inhomogeneity for the dynamics of ULF Alfvén waves and FACs has been emphasized in several studies (e.g., Mishin & Förster, 1995; Streltsov et al., 2012). To investigate how the transverse inhomogeneity in the ionospheric conductivity and the electric field modifies the nonlinear development of the instability, simulations with different plasma cavities have been performed. In all of them, the magnitude of the plasma density is 10^4 cm^{-3} at the center of the cavity and $5 \times 10^4 \text{ cm}^{-3}$ outside the cavity ($\kappa = 5$). The corresponding electric field has a Gaussian-like shape with maximum of 10 mV/m. The simulations were initiated with the same density disturbance as the one used in the homogeneous case in the center of the cavities. Three cavities with $\Delta L = (L_2 - L_1)$, $\Delta L = (L_2 - L_1)/2$, and $\Delta L = (L_2 - L_1)/4$ have been considered.

The results from these simulations are illustrated in Figure 4. In particular, Figures 4a and 4b show the magnitude of the background electric field and plasma density used in the simulation with $\Delta L = (L_2 - L_1)/2$. Figure 4c shows a snapshot of the parallel current density taken from this simulation at $t = 3,011.1 \text{ s}$. Figures 4d–4f show profiles of the background plasma density and the electric field in the ionosphere used in simulations with different cavities. They also show magnitudes of j_{\parallel} in the ionosphere taken from the corresponding simulations at $t = 3,090.3 \text{ s}$, $t = 3,011.1 \text{ s}$, and $t = 2,884.3 \text{ s}$. These moments of time were chosen well after the instability reaches a saturated, strongly nonlinear stage. In all three cases, the instability develops with the same linear growth rate and saturates at the same magnitudes of the parallel current density.

Figure 4 shows that the main role of the cavity is to confine the development of the instability near the cavity center, where the conductivity has its minimum and the electric field has its maximum, in other words, where the conditions for the instability are satisfied. The main difference between the FACs developed in the cavity and in the homogeneous ionosphere is the perpendicular size of the currents. These sizes are less inside the

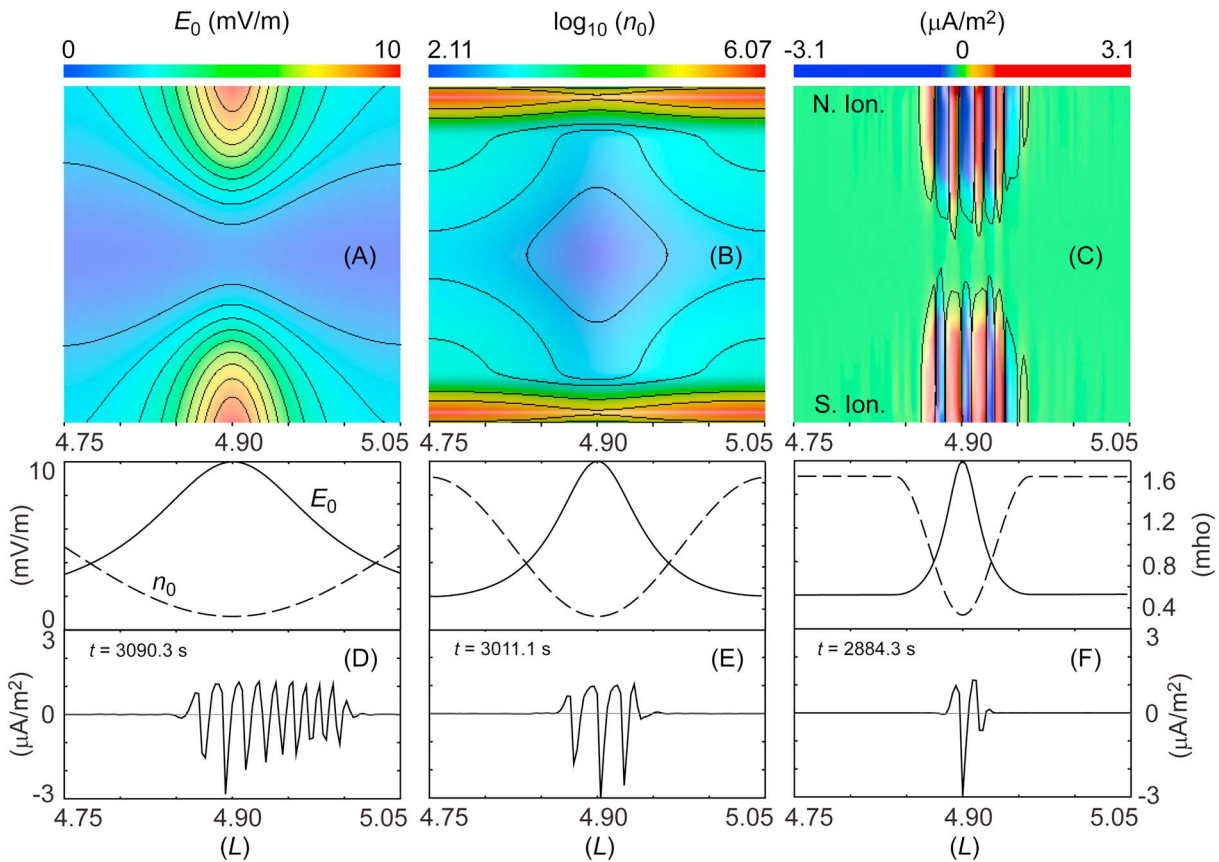


Figure 4. (a) Background electric field, (b) the logarithm of the background plasma density, and (c) the snapshot of $j_{||}$ at time $t = 3,011.1$ s in the simulations with $\Delta L = (L_2 - L_1)/2$. (d–g) Profiles of the background electric field, conductivity, and the parallel current density in the southern hemisphere in simulations with $\Delta L = (L_2 - L_1)$, $\Delta L = (L_2 - L_1)/2$, and $\Delta L = (L_2 - L_1)/4$.

cavity than in the homogeneous plasma, which means that the transverse gradients in the background plasma and the electric field change the perpendicular sizes of the generated structures.

The effects of the cavity on the development of the IFI had been investigated in more detail by Streltsov et al. (2012). They used the same model as the one considered in this study and implemented it in the same part of the magnetosphere, but the focus of their investigation was on the magnetic fields and frequencies of the ULF waves generated by the IFI in different cavities. Despite of the small difference of the background parameters used in their study compared with the ones used in this paper, the major conclusions about the qualitative behavior of the IFI in cavities from both studies are quite consistent.

To understand the effect of the amplitude of the background electric field on the IFI development, simulations with an electric field with a maximum magnitude 20 mV/m in the ionosphere have been performed. The first conclusion from these simulations is that the large electric field causes large FACs. In the case of a 20-mV/m field, the maximum amplitude of currents reaches $6.2 \mu\text{A}/\text{m}^2$, whereas in the case of a 10-mV/m field, the maximum amplitude of current was $\approx 3.1 \mu\text{A}/\text{m}^2$. The second conclusion is that the downward current channels are broader in the 20-mV/m case than in the 10-mV/m case.

The last result obtained in the simulations relates to the effect of the amplitude of the background ionospheric density/conductivity on the IFI development. The simulations show that density affects the linear growth rate of the instability: specifically, that a larger density causes a smaller growth rate. For example, IFI driven by 10-mV/m electric field inside a cavity with the minimum density $1.5 \times 10^4 \text{ cm}^{-3}$ (corresponding to $\Sigma_p = 0.50$ mho) has a growth rate $1.5 \times 10^{-3} \text{ s}$, whereas IFI driven by the same electric field in the cavity with the minimum density $1.0 \times 10^4 \text{ cm}^{-3}$ (corresponding to $\Sigma_p = 0.33$ mho) has the growth rate $3.2 \times 10^{-3} \text{ s}$. This result is consistent with the analytical estimates of the linear growth rate given by Trakhtengertz and Feldstein

(1991), Lysak (1991), and Pokhotelov et al. (2000) and one more time demonstrates that the instability will not develop when the ionospheric conductivity is high.

4. Conclusions

This paper presents results from simulations of a two-fluid MHD model describing magnetosphere-ionosphere interaction conducted by ULF electromagnetic waves and FACs at high latitudes. The goal of this study is to explain self-consistent formation of the FAC system with the characteristic features of the black aurora.

Results from this study suggest that the black aurora is produced by the strongly nonlinear IFI developed simultaneously in two magnetically conjugate hemispheres. The favorable conditions for the development of the black aurora include a relatively homogeneous and relatively stationary state of the plasma density and the electric field in the ionosphere. The electric field should be in the range of 10–20 mV/m. (A larger field will cause very rapid dynamics of small-scale structures.) The background ionospheric conductivity should be less than 0.3–0.5 mho. (Larger conductivity would not allow the IFI driven by 10–20-mV/m electric field to reach the nonlinear stage during any reasonable time interval.) These conditions promote the development of significant (by a factor of 3 or more) differences in spatial sizes and amplitudes between the upward and downward FAC interacting with the ionosphere, which explain the main observational features of the black aurora.

5. Data Availability

The images of the black aurora (Figure 1), the executable code used in the simulations, the data files used to run the code, and the results from the simulation shown in Figure 2 are available from Figshare.com (<https://doi.org/10.6084/m9.figshare.7066544>).

Acknowledgments

Author acknowledges fruitful discussions of the results with colleagues at the International Space Science Institute, Bern, Switzerland. This research had been supported by the National Academy of Sciences at Space Vehicles Directorate, Air Force Research Laboratory, Kirtland AFB.

References

- Atkinson, G. (1970). Auroral arcs: Result of the interaction of a dynamic magnetosphere with the ionosphere. *Journal of Geophysical Research*, *75*, 4746–4755.
- Chmyrev, V. M., Bilichenko, S. V., Pokhotelov, O. A., Marchenko, V. A., Lazarev, V. I., Streltsov, A. V., & Steflo, L. (1988). Alfvén vortices and related phenomena in the ionosphere and the magnetosphere. *Physica Scripta*, *38*, 841–854.
- Cummings, W. D., O'Sullivan, R. J., & Coleman, P. J. Jr. (1969). Standing Alfvén waves in the magnetosphere. *Journal of Geophysical Research*, *74*, 778–793.
- Goertz, C., & Boswell, R. (1979). Magnetosphere-ionosphere coupling. *Journal of Geophysical Research*, *84*, 7239–7246.
- Gustavsson, B., Kosch, M. J., Senior, A., Kavanagh, A. J., Brandstrom, B. U. E., & Blixt, E. M. (2008). Combined EISCAT radar and optical multispectral and tomographic observations of black aurora. *Journal of Geophysical Research*, *113*, A06308. <https://doi.org/10.1029/2007JA012999>
- Hasegawa, A. (1976). Particle acceleration by MHD surface wave and formation of aurora. *Journal of Geophysical Research*, *81*, 5083–5090.
- Lysak, R. L. (1991). Feedback instability of the ionospheric resonant cavity. *Journal of Geophysical Research*, *96*, 1553–1568.
- Lysak, R. L., & Dum, C. T. (1983). Dynamics of magnetosphere-ionosphere coupling including turbulent transport. *Journal of Geophysical Research*, *88*, 365–380.
- Lysak, R. L., & Song, Y. (2002). Energetics of the ionospheric feedback interaction. *Journal of Geophysical Research*, *107*(A8), 1160. <https://doi.org/10.1029/2001JA000308>
- Marklund, G., Blomberg, L., Falthammar, C.-G., & Lindqvist, P.-A. (1994). On intense diverging electric fields associated with black aurora. *Geophysical Research Letters*, *21*, 1859–1862.
- Marklund, G., Ivchenko, N., Karlsson, T., Fazakerley, A., Dunlop, M., Lindqvist, P.-A., et al. (2001). Temporal evolution of the electric field accelerating electrons away from the auroral ionosphere. *Nature*, *414*, 724–727.
- Marklund, G., Karlsson, T., & Clemmons, J. (1997). On low-altitude particle acceleration and intense electric fields and their relationship to black aurora. *Journal of Geophysical Research*, *102*(A8), 17,509–17,522.
- Marklund, G., Sadeghi, S., Karlsson, T., Lindqvist, P.-A., Nilsson, H., Forsyth, C., et al. (2011). Altitude distribution of the auroral acceleration potential determined from Cluster satellite data at different heights. *Physical Review Letters*, *106*, 055002. <https://doi.org/10.1103/PhysRevLett.106.055002>
- Mishin, E. V., & Förster, M. (1995). "Alfvénic shocks" and low-altitude auroral acceleration. *Geophysical Research Letters*, *22*, 1745–1748.
- Miura, A., & Sato, T. (1980). Numerical simulation of global formation of auroral arcs. *Journal of Geophysical Research*, *85*, 73–91.
- Pokhotelov, O., Khrushev, V., Parrot, M., Senchenkov, S., & Pavlenko, V. (2001). Ionospheric Alfvén resonator revisited: Feedback instability. *Journal of Geophysical Research*, *106*, 25,813–25,824.
- Pokhotelov, O., Pokhotelov, D., Streltsov, A., Khrushev, V., & Parrot, M. (2000). Dispersive ionospheric Alfvén resonator. *Journal of Geophysical Research*, *105*, 7737–7746.
- Polyakov, S. V., & Rapoport, V. O. (1981). The ionospheric Alfvén resonator. *Geomagnetism and Aeronomy*, *21*, 816–822.
- Russell, A., Wright, A., & Streltsov, A. (2013). Production of small-scale Alfvén waves by ionospheric depletion, ionospheric feedback mechanism and phase mixing. *Journal of Geophysical Research: Space Physics*, *118*, 1450–1460. <https://doi.org/10.1002/jgra.50168>
- Samson, J. C., Wallis, D. D., Hughes, T. J., Greutzberg, F., Ruohoniemi, J. M., & Greenwald, R. A. (1992). Substorm intensifications and field line resonances in the nightside magnetosphere. *Journal of Geophysical Research*, *97*, 8495–8518.
- Sato, T. (1978). A theory of quiet auroral arcs. *Journal of Geophysical Research*, *83*, 1042–1048.

- Stasiewicz, K., Bellan, P., Chaston, C., Kletzing, C., Lysak, R., Maggs, J., et al. (2000). Small scale Alfvénic structure in the aurora. *Space Science Reviews*, 92, 423–533.
- Streltsov, A., Jia, N., Pedersen, T., Frey, H., & Donovan, E. (2012). ULF waves and discrete aurora. *Journal of Geophysical Research*, 117, A09227. <https://doi.org/10.1029/2012JA017644>
- Streltsov, A., & Lotko, W. (2005). Ultra-low-frequency electrodynamics of the magnetosphere-ionosphere interaction. *Journal of Geophysical Research*, 110, A08203. <https://doi.org/10.1029/2004JA010764>
- Streltsov, A., & Marklund, G. (2006). Divergent electric fields in downward current channels. *Journal of Geophysical Research*, 111, A07204. <https://doi.org/10.1029/2005JA011196>
- Streltsov, A., Pedersen, T., Mishin, E., & Snyder, A. (2011). Ionospheric feedback instability and substorm development. *Journal of Geophysical Research*, 115, A07205. <https://doi.org/10.1029/2009JA014961>
- Sydorenko, D., & Rankin, R. (2017). The stabilizing effect of collision-induced velocity shear on the ionospheric feedback instability in Earth's magnetosphere. *Geophysical Research Letters*, 44, 6534–6542. <https://doi.org/10.1002/2017GL073415>
- Trakhtengertz, V., & Feldstein, A. (1981). Influence of Alfvén velocity inhomogeneous profile on magnetospheric convection stratification. *Geomagnetizm i Aehronomiya*, 21, 951–953.
- Trakhtengertz, V. Y., & Feldstein, A. Y. (1984). Quiet auroral arcs: Ionospheric effect of magnetospheric convection stratification. *Planetary and Space Science*, 32, 127–134.
- Trakhtengertz, V., & Feldstein, A. (1991). Turbulent Alfvén boundary layer in the polar ionosphere. 1. Excitation conditions and energetics. *Journal of Geophysical Research*, 96, 19,363–19,374.
- Trondsen, T., & Cogger, L. (1997). High-resolution television observations of black aurora. *Journal of Geophysical Research*, 102, 363–378.
- Watanabe, T., Oya, H., Watanabe, K., & Sato, T. (1993). Comprehensive simulation study on local and global development of auroral arcs and field-aligned potentials. *Journal of Geophysical Research*, 98, 21,391–21,407.